Supporting Information

Versatile MOFs with dual-enzyme-mimetic activities for cancer hypoxia relief and assisted photodynamic therapy upon fluorescence imaging

Xiaotong Li[a], Haoyun Shi[a], Zimeng Zhou[a], Linshan Jia[a], Xiaohong Hou[b*]

a School of Pharmacy, Shenyang Pharmaceutical University, Shenyang, Liaoning Province, 110016, PR China

b School of Pharmaceutical Engineering, Shenyang Pharmaceutical University, Shenyang, Liaoning Province, 110016, PR China

** Corresponding author. School of Pharmaceutical Engineering, Shenyang Pharmaceutical University, Shenyang, Liaoning Province, 110016, PR China.*

Email address of the corresponding author: syphu_houxiaohong@163.com (X. Hou).

Phone numbers of the corresponding author: 024-43520212 (X. Hou).

Content

1. Main reagents

Text S1. Main reagents

All reagents were commercially purchased and used directly without purification. Zirconium Oxychloride Octahydrate ($ZrOCl_2 \cdot 8H_2O$), L(+)-Arginine, Cerium (III) nitrate hexahydrate($Ce(NO_3)_3 \cdot 6H_2O$) and Dichloroacetic acid were purchased from Aladdin Reagent Company (Shanghai, China). 1,3-diphenylisobenzofuran (DPBF), 3-(4,5-dimethylthiazol-2-yl)-2,5-diphenyl-tetrazolium bromide (MTT), sodium hypochlorite (NaClO) and 5,5'-(anthracene-9,10-dial)−diisophthalicacid(H_4adip) were gained from Macklin Biochemical Co., Ltd (Shanghai, China). Dulbecco's modified Eagle's medium (DMEM), phosphate buffer saline (PBS),2-(4-Amidinophenyl)-6-indolecarbamidine dihydrochloride (DAPI), Calcein-AM/PI double stain kit and cellular singlet oxygen detection assay kit (DCFH-DA) were purchased from Meilun Biotechnology Co., Ltd (Dalian, China). Dimethyl sulfoxide (DMSO), N, N-dimethylformamide (DMF), and ethanol were purchased from Fuyu Fine Chemicals Co., Ltd (Tianjin, China). Other chemicals and solvents were of analytical grade.

2. Main instruments

Text S2. Main instruments

UV-vis spectra were conducted on a Shimadzu UV-2450 spectrophotometer. Fluorescence spectra were performed with a Yidian 970CRT spectrophotometer. Confocal laser scanning microscopy (CLSM) images were obtained using a Nikon C2 confocal laser scanning microscope. Inverted fluorescence imaging was detected by Primovert inverted microscope. The generated oxygen was determined with the HI9146 portable dissolved oxygen meter (Hanna Instruments, Italy). MTT cytotoxicity assay was performed on a multi-mode microplate reader (Thermo Varioskan Flash, USA).

3. Loading and release of H_4adip

Text S3. Loading and release of H_4adip

3.1 Preparation of standard curve

A stock solution of H_4adip with a concentration of 1 mg·mL^{-1} was prepared in DMF as the solvent and dispersed by ultrasonication. Appropriate volumes of the stock solution were accurately measured, transferred into volumetric flasks, diluted to the mark with ethanol, and shaken well to obtain a series of standard solutions with concentrations of 5, 10, 20, 40, 50, 60, and 80 μg·mL^{-1}. The absorbance of each solution was measured at 373 nm. A standard curve was constructed by linear regression with concentration as the abscissa and the mean absorbance as the ordinate.

3.2 Determination of loading capacity

A DMF solution of H_4adip (5 mL, 24 mg·mL^{-1}) was added dropwise to an ethanol solution of PCN-222 (30 mL, 2 mg·mL^{-1}). The mixture was then stirred continuously in the dark at 60°C for 24 h. Collect (200 μL) of the reaction solution were collected at 0, 1, 2, 3, 4, 8, 12, and 24 h, diluted with anhydrous ethanol to 3 mL, and thoroughly mixed. The UV absorbance of each sample was measured at 373 nm, and each time point was sampled and measured in triplicate. The average absorbance values were substituted into the standard curve to calculate the mass of unloaded H_4adip in the solution, and the loading capacity and loading efficiency were further determined.

3.3 Investigation of release behavior

HPC (2 mg·mL^{-1}) was added to water, PBS (pH 6.5), and RPMI-1640 medium, respectively, and mixed thoroughly to form the release systems. Each release system was incubated under identical conditions, and an equal volume of solution was added immediately after sample collection. Samples were collected at 0, 12, 24, 36, 48, 60, and 72 h, and

centrifuged at 10,000 rpm for 10 min. The supernatants were filtered, and the filtrates were collected. The absorbance of the filtrates at 373 nm was measured using a UV-vis spectrophotometer. The mass of H_4adip released into different mediums was calculated by substituting the absorbance values into the standard curve.

4. Biological safety

Text S4. Biological safety

MCF-7 cells were inoculated in 96-well plates, and 200 μL of cell suspension was added to each well, and three replicates per group were established. Blank control group was added with equal amount of PBS and incubated in a cell culture incubator for 24 h. Subsequently, the original medium was replaced with HP and HPC mixes at different concentrations (0, 6.25, 12.5, 25, 50, 100, and 200 $\mu g \cdot mL^{-1}$). After 12 h of incubation, the culture was washed with PBS and 100 μL of new medium was added to each well with 20 μL of MTT solution (5 $mg \cdot mL^{-1}$). After continuing the incubation for 4 h, the medium was removed, 150 μL DMSO was added to each well, and the OD value at 490 nm was measured using an enzyme marker and the cell viability was calculated. The biocompatibility assay for 293T cells, HepaRG hepatocytes, and HK-2 renal cells was performed in the same way as described above. The cell viability was calculated as follows:

The biocompatibility assay of 293T cells was performed in the same way as described above. The cell viability was calculated as follows:

$$Cell\ Viability\ (\%) = \frac{OD_{sample} - OD_{blank}}{OD_{control} - OD_{blank}} \times 100\%$$

where OD_{sample}, OD_{blank}, and $OD_{control}$ represent the optical density values of the experimental, blank, and control groups, respectively.

To assess the tumor specificity and off-target toxicity risk of the HPC nanoplatform, we calculated the ratio of tumor cell viability to normal cell viability.

5. The structure of H_4adip

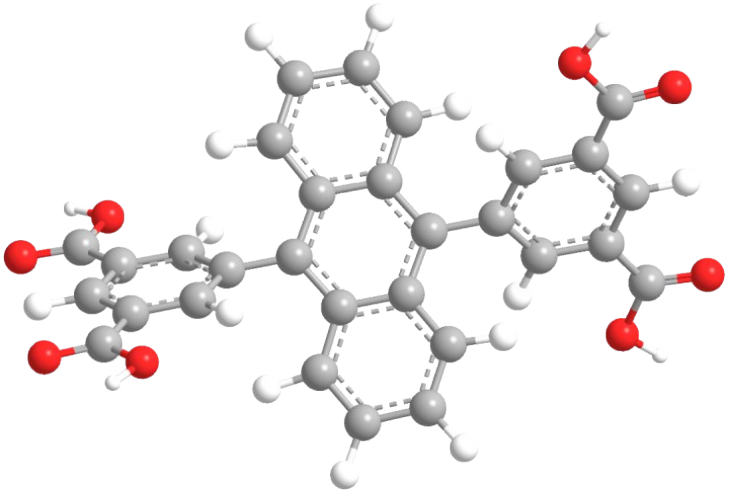

Fig. S1. The structure of H_4adip.

6. The result of loading and release of H_4adip

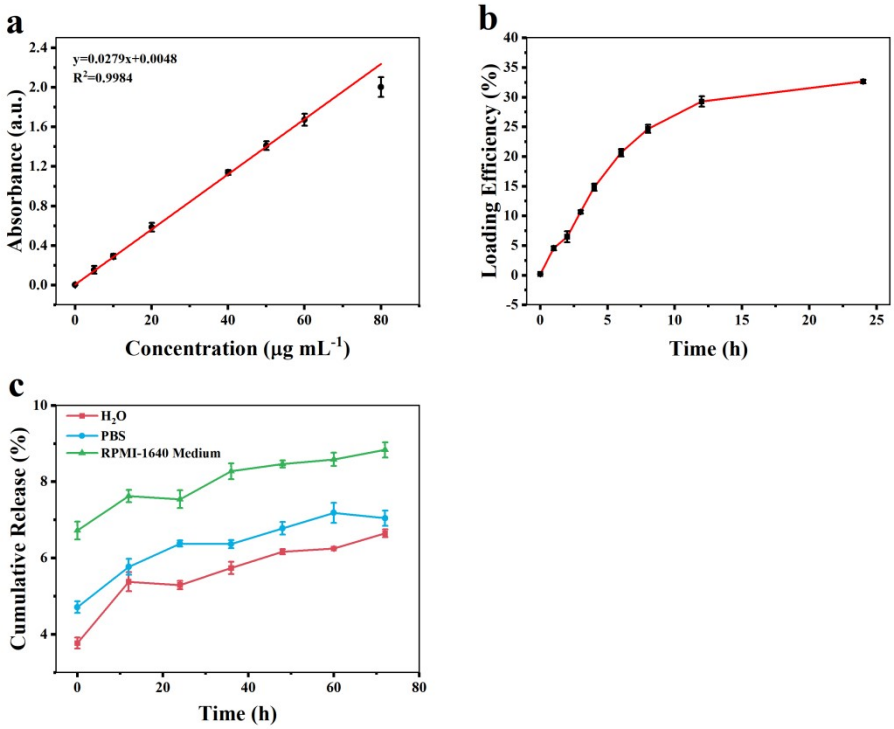

Fig. S2. (a) Standard calibration curve of H_4adip in ethanol (λ = 373 nm). (b) Calculated loading efficiency of H_4adip. (c) Cumulative release profile of H_4adip from HPC at different mediums.

7. Particle size distribution profile of HPC.

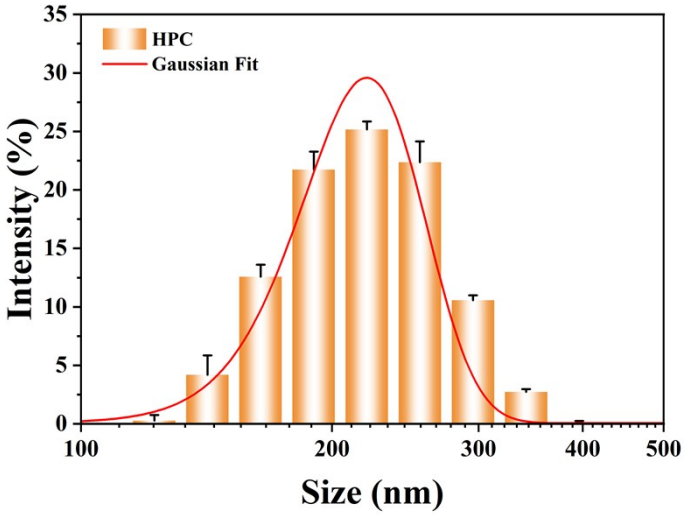

Fig. S3. Particle size distribution profile of HPC.

8. EDS spectrum of HPC

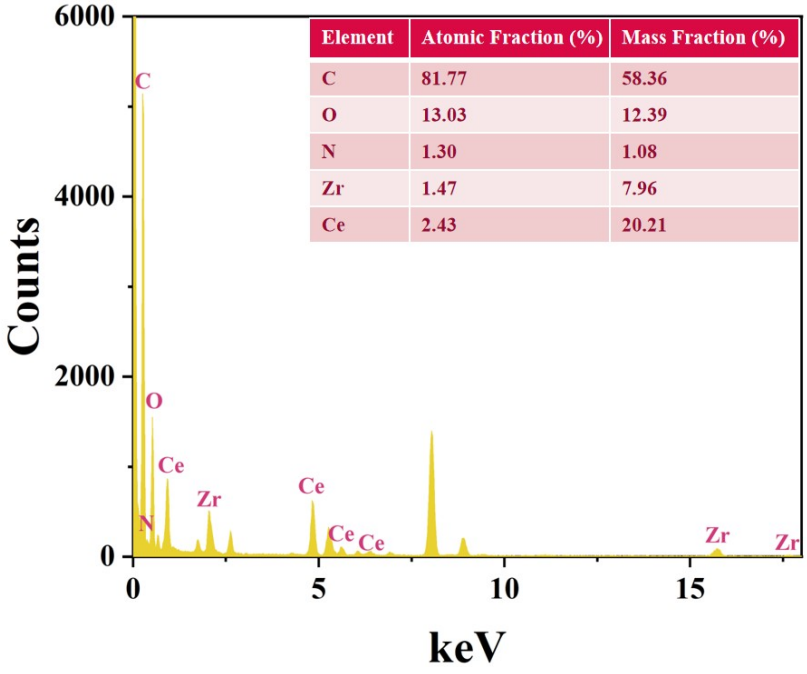

Fig. S4. EDS spectrum of HPC.

9. Photos of H_4adip, PCN-222, HP, and HPC dispersed in an aqueous solution

Fig. S5. Photos of H_4adip, PCN-222, HP, and HPC dispersed in an aqueous solution during HPC synthesis process.

10. N_2 adsorption/desorption test

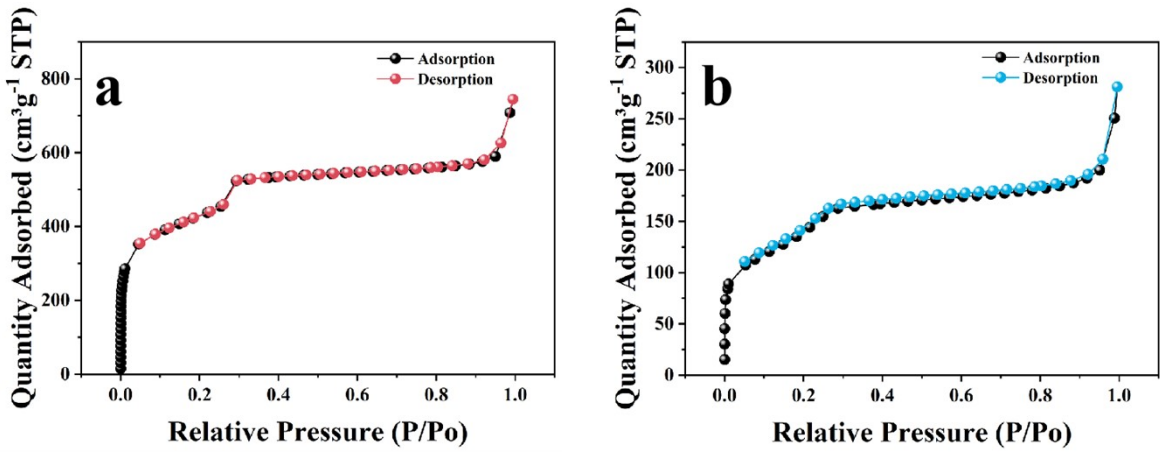

Fig. S6. N_2 adsorption/desorption isotherms of PCN-222 (a) and HP (b).

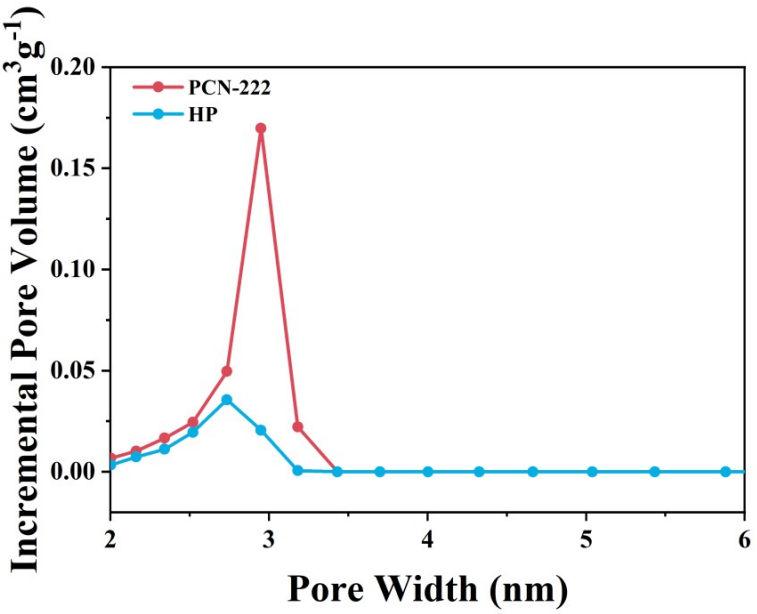

Fig. S7. Pore size distribution of PCN-222 and HP nanoparticles.

Table. S1. Specific surface area and pore volume of PCN-222 and H_4adip@PCN-222.

Material	BET Surface Area (m^2 g^{-1})	Pore Volume (cm^3 g^{-1})
PCN-222	1546.70	1.15
H_4adip@PCN-222	508.03	0.43

11. Fluorescence spectra of PCN-222, H_4adip, and HPC

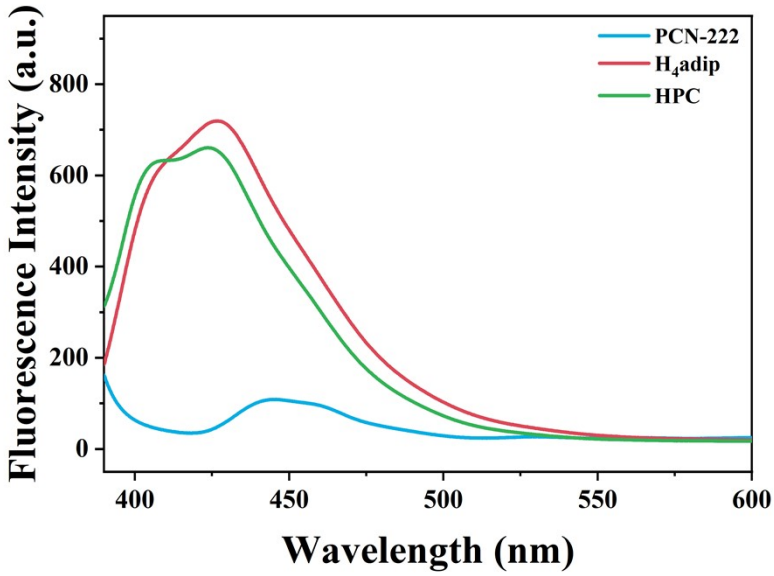

Fig. S8. Fluorescence spectra of PCN-222, H_4adip, and HPC (λ_{ex}=379 nm).

12. The CAT-like activity and enzyme kinetic properties of HPC

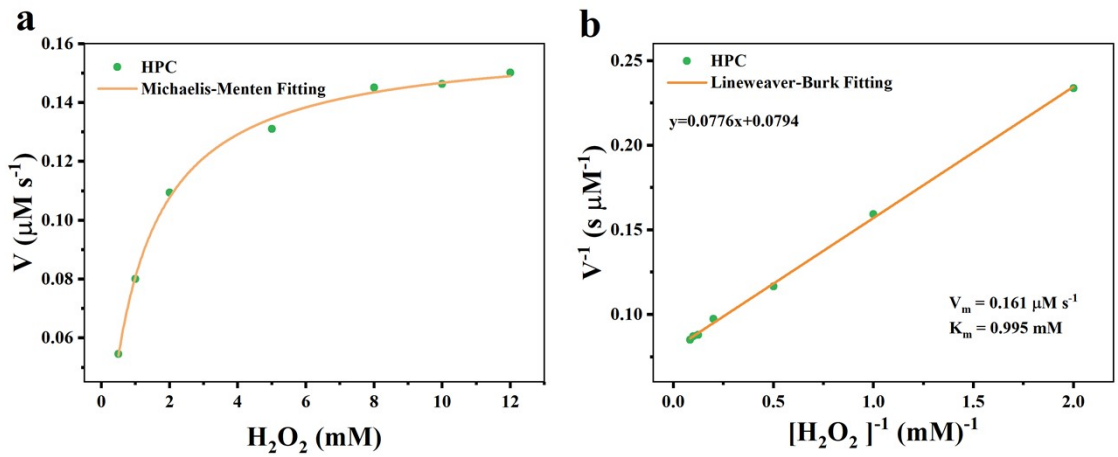

Fig. S9. (a) Michaelis-Menten kinetic fitting for CAT-like activity of HPC at different H_2O_2 concentrations (0.5 - 12 mM). (b) Lineweaver-Burk plot of CAT-like activity of HPC derived from the Michaelis-Menten equation.

13. Effect of pH on the CAT-like activity of HPC

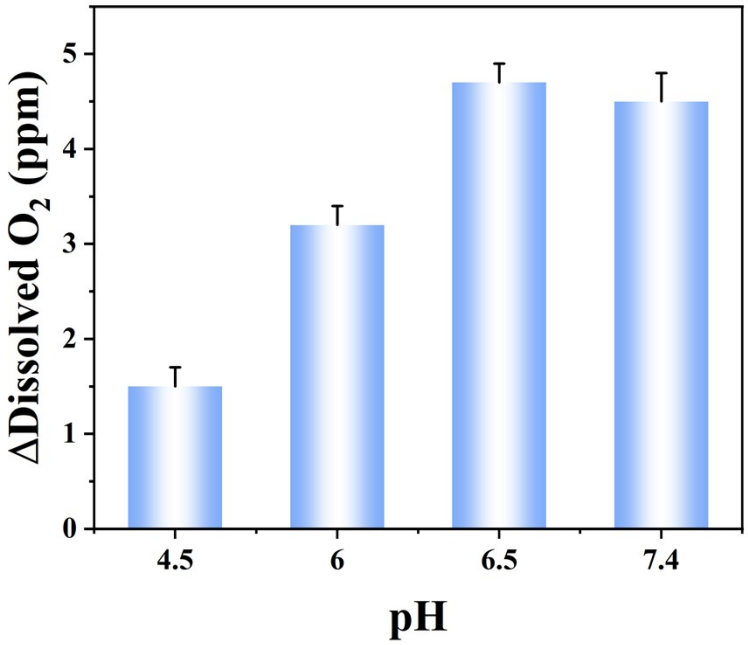

Fig. S10. The amount of O_2 generated from H_2O_2 catalyzed by HPC under different pH.

14. Photos of oxTMB of HPC with H_2O_2

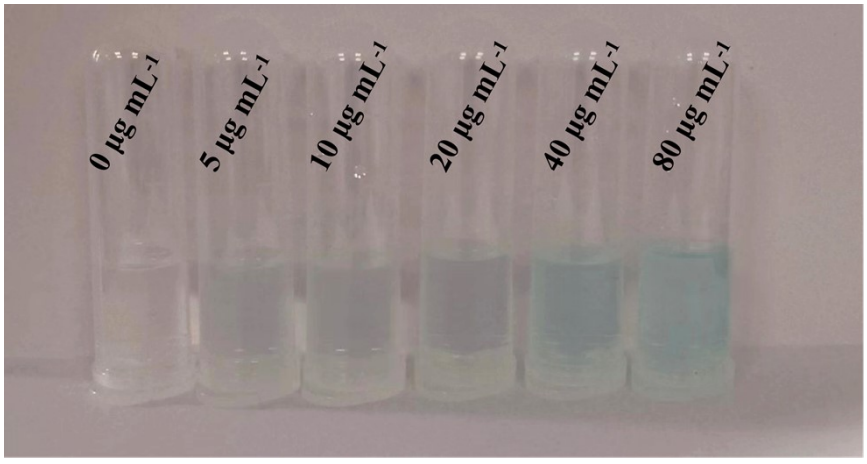

Fig. S11. Photos of oxTMB of different concentrations of HPC (0, 5, 10, 20, 40, and 80 μg·mL^{-1}) with H_2O_2 (10 mM).

15. The POD-like activity and enzyme kinetic properties of HPC

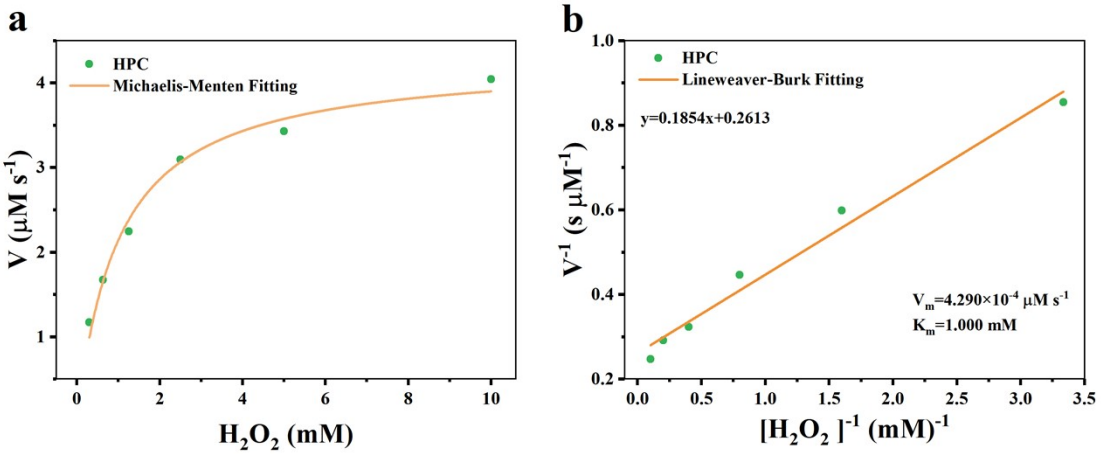

Fig. S12. (a) Michaelis-Menten kinetic fitting for POD-like activity of HPC at different H_2O_2 concentrations (0.3 - 10 mM). (b) Lineweaver-Burk plot of POD-like activity of HPC derived from the Michaelis-Menten equation.

16. Effect of pH on the POD-like activity of HPC

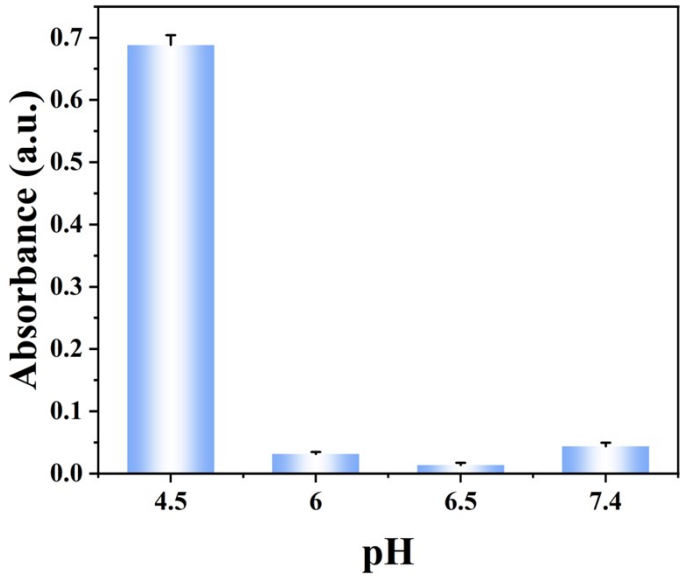

Fig. S13. The absorbance at 655 nm of oxTMB catalyzed by HPC under different pH.

17. UV-vis absorbance spectral changes of DPBF over time after different treatments

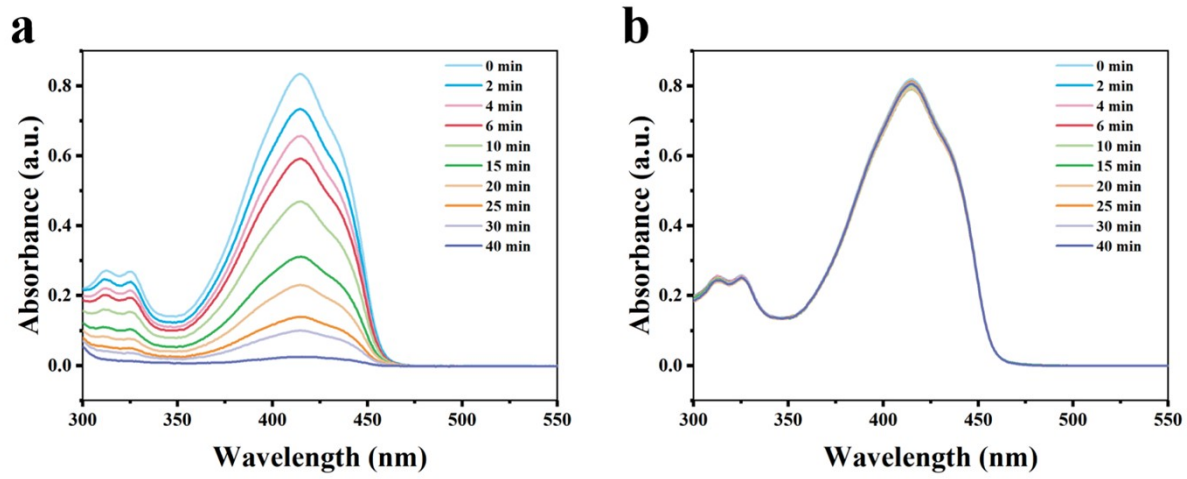

Fig. S14. UV-vis absorption spectra changes of DPBF over time with (a) and without (b) light irradiation in the presence of HPC.

18. The $^1O_2$ generating ability of CeO_2 nanozyme

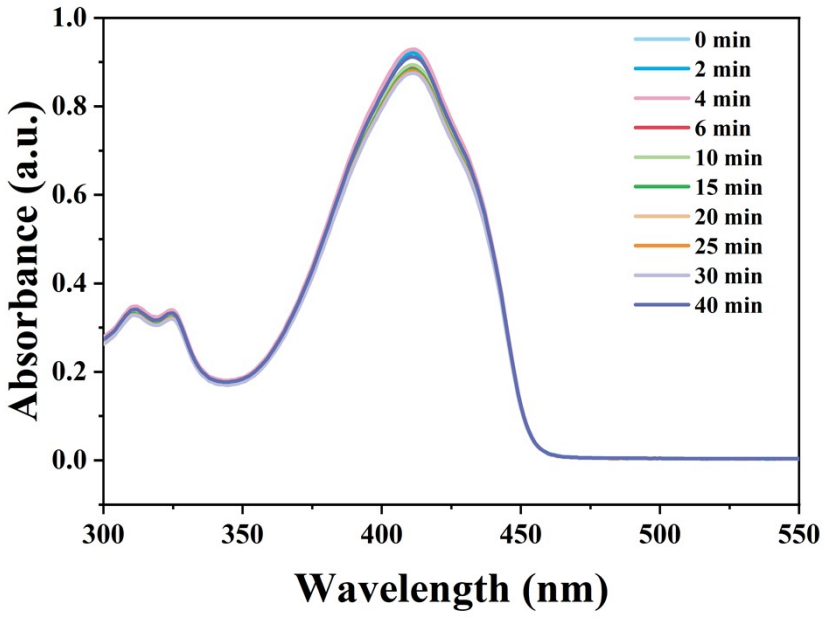

Fig. S15. UV-vis absorption spectrum changes of DPBF over time with light irradiation in the presence of nano CeO_2.

19. Fluorescence spectral changes of HPC over time after different treatments

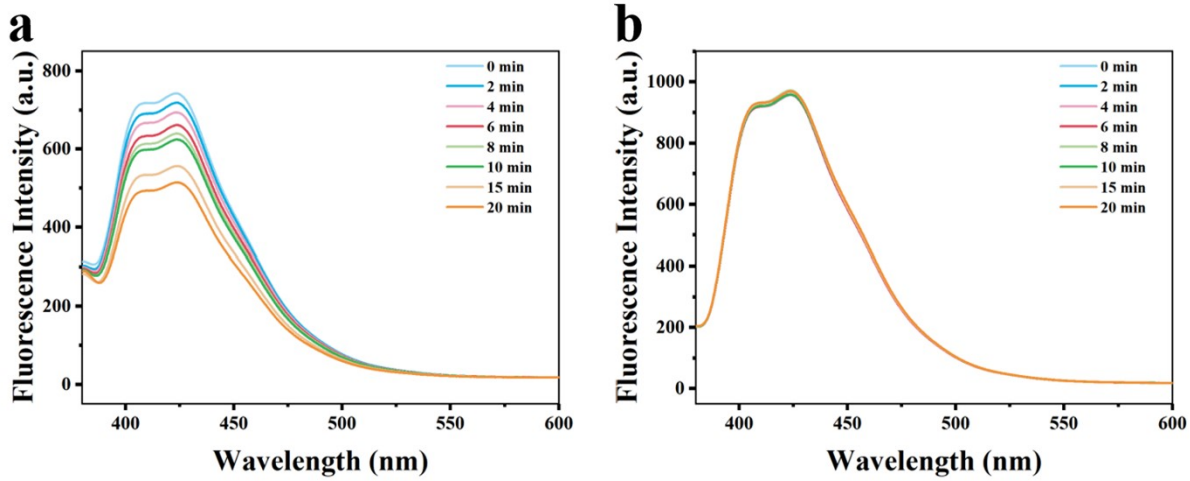

Fig. S16. Fluorescence spectral changes of HPC over time (a) with or (b) without light irradiation under normoxic conditions.

20. Schematic diagram of the reaction between H_4adip and $^1O_2$

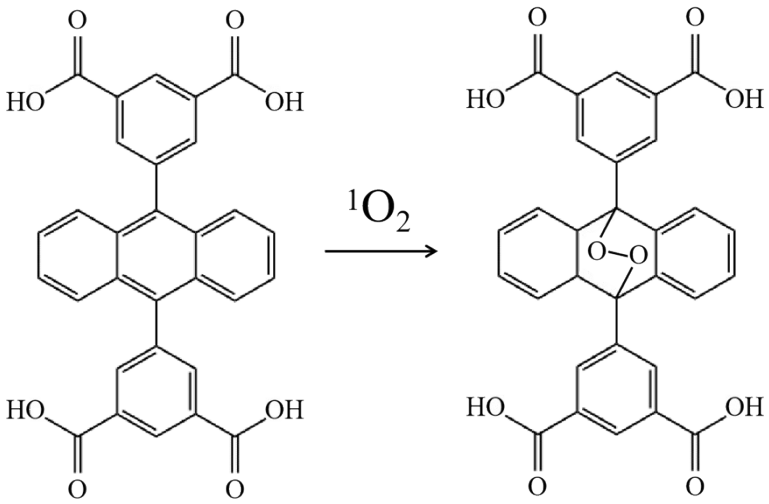

Fig. S17. Schematic diagram of the reaction between H_4adip and $^1O_2$.

21. Validation of HPC sensitivity for $^1O_2$ detection using the Na_2MoO_4/H_2O_2 system

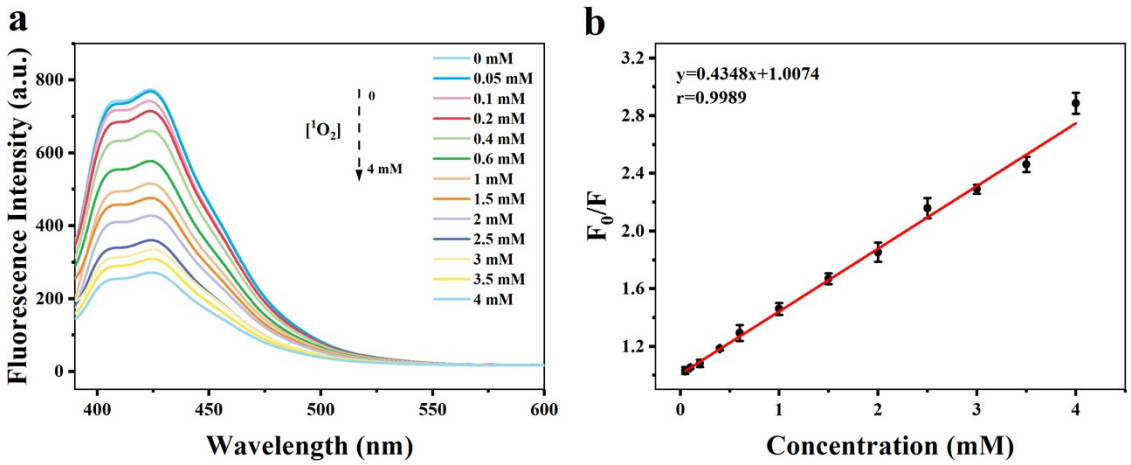

Fig. S18. (a) Fluorescence spectrum changes of HPC in the presence of $^1O_2$ with concentrations from 0 to 4 mM (λ_{ex} = 379 nm, λ_{em} = 390-600 nm). (b) F_0/F changes of HPC in the presence of $^1O_2$ with concentrations from 0.05 to 4 mM.

22. The result of biological safety

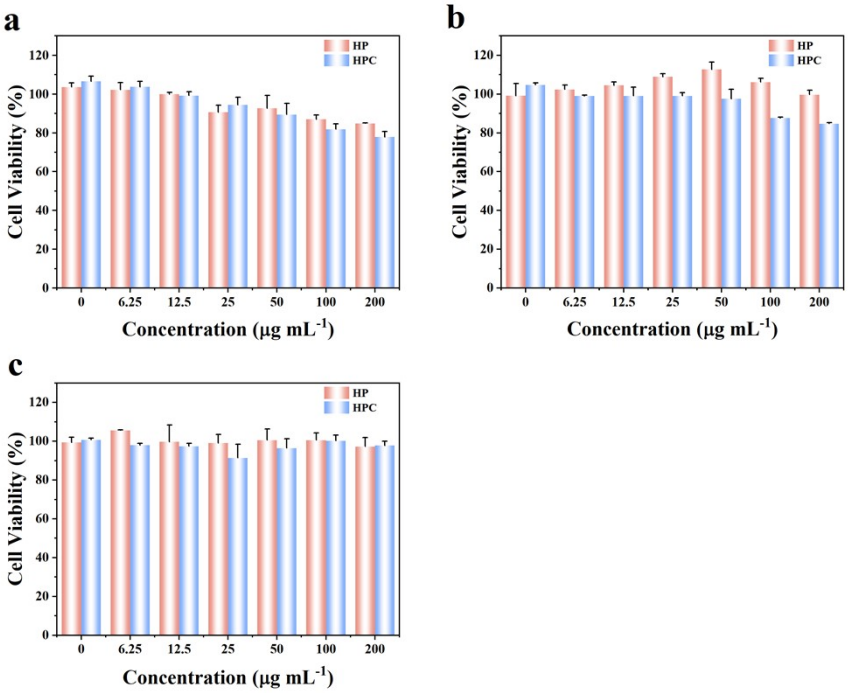

Fig. S19. Cell viability of (a) HepaRG hepatocytes, (b) HK-2 renal cells, and (c) 293T cells treated with different concentrations of HP or HPC in the absence of light irradiation.

23. Cytotoxicity of H_2O_2

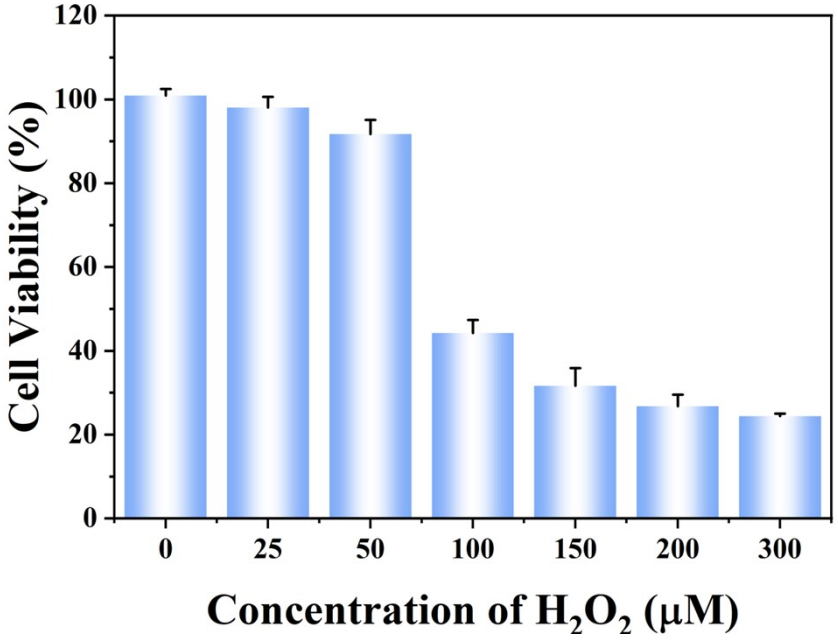

Fig. S20. Viability of MCF-7 cells incubated with H_2O_2.

24. Cell viability of MCF-7 cells under different irradiation time

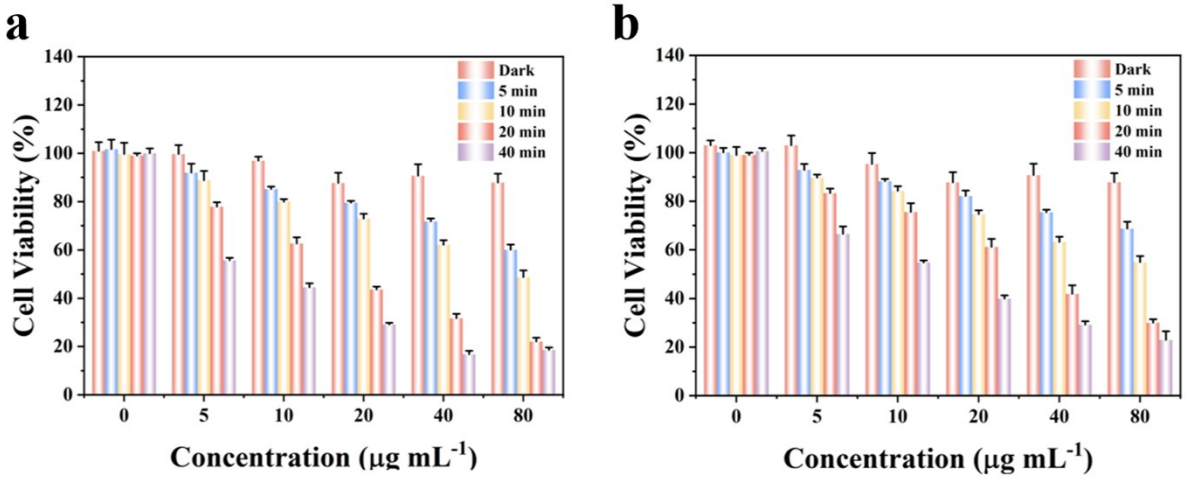

Fig. S21. Cell viability of MCF-7 cells treated with (a) HPC or (b) HP with different concentrations under different laser irradiation times.

25. Cytotoxicity of ·OH

To evaluate the killing effect of ·OH catalytically produced by HP and HPC on tumor cells, the experimental procedure was similar to the cytobiocompatibility assay. First, cells were inoculated into 96-well plates at a density of 1×10^3 cells per well and 200 μL per well, with three replicates per group, and incubated in an incubator for 24 h. After pouring off the original medium, HP and HPC mixtures with concentrations of 0, 5, 10, 20, 40 and 80 μg·mL^{-1} were added, and the blank control group was added with equal amounts of PBS. 12 h later, 50 μM H_2O_2 was added to each well, and the cells were incubated for 4 h for comparison of MTT effects.

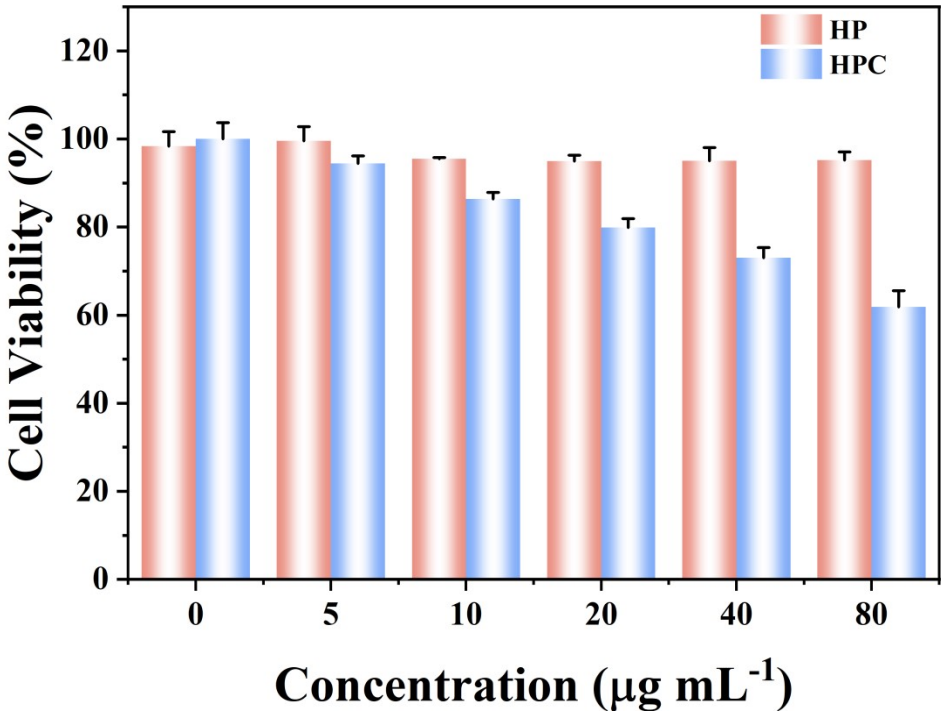

Fig. S22. Cell viability of MCF-7 cells treated with different concentrations of HPC and H_2O_2 (50 μM).

26. Live/dead staining

MCF-7 cells (5×10^4 cells per well) were seeded and cultured in 24-well plates for 24 h at 37℃ Next, cells were grouped and treated with HP+H_2O_2, HPC+H_2O_2, HP+laser, HPC+laser, HP+H_2O_2+laser, and HPC+H_2O_2+laser. After washing several times with PBS, calcein-AM (2 μmol L^{-1}) and PI (4 μmol L^{-1}) were added to stain the cells. Fluorescence images were taken using an inverted fluorescence microscope.

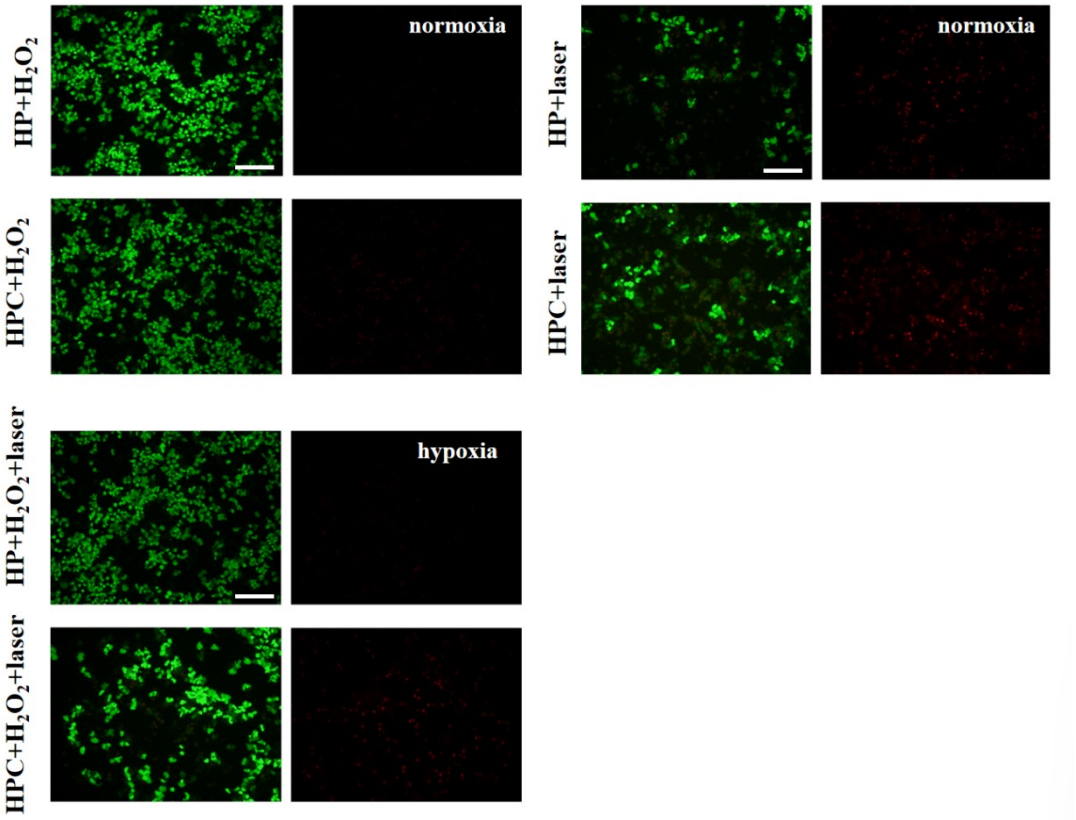

Fig. S23. Live/dead cell assay for MCF-7 cells treated with HP or HPC, scale bar = 100 μm. (green: live cells, red: dead cells).

27. Recently reported nanomaterials-based methods for determination of $^1O_2$

Table. S2. An overview on recently reported nanomaterials-based methods for determination of $^1O_2$.

Probe/Material	$^1O_2$-trap	Linear range	LOD	Ref.
EuPS@AnC/ZIF-8 NPs	Anthracene	0.5-200 μM	43 nM	1
ICG-DPBF-PFP/conjugated polymer hybrid NPs	DPBF	0-2 mM	28 μM	2
PEG-AuNPs-PCN-224/DPA	Anthracene	0.1-3.5 μM	35.8 μM	3
Fe_3O_4@PCN-224@CaO_2-ABDA	Anthracene	0.15-2.5 mM	60.6 μM	4
DSPE-SS-PEG_{2k}@TPP@TCPP@DPA-MOF	Anthracene	0-4 mM	63.9 μM	5
TCPP@DPA-MOF-Pt NPs	Anthracene	0.2-4 mM	64.9 μM	6
H_4adip@PCN-222@CeO_2	Anthracene	0.05-4 mM	43.4 μM	This work

References

1. J. Gao, C. Wang and H. Tan, *Journal of Materials Chemistry B*, 2017, **5**, 9175–9182.
2. X.-h. Wang, Y.-x. Yu, K. Cheng, W. Yang, Y.-a. Liu and H.-s. Peng, *Microchimica Acta*, 2019, **186**, 842.
3. L. Yu, L. Feng, L. Xiong, S. Li, Q. Xu, X. Pan and Y. Xiao, *ACS Applied Materials & Interfaces*, 2021, **13**, 11646–11656.
4. Y. Yang, N. Li, Y. Zhu, J. Li, S. Li and X. Hou, *Talanta*, 2023, **259**, 124493.
5. S. Li, F. Yang, Y. Wang, L. Jia and X. Hou, *Materials Horizons*, 2023, **10**, 5734–5752.

6. T. Entradas, S. Waldron and M. Volk, *Journal of Photochemistry and Photobiology B: Biology*, 2020, **204**, 111787.